

LES – VOF simulation of gas-jet wiping: confrontation to experiments

*A Gosset**, *D Lacanette***, *S Vincent***, *E Arquis***, *J–M Buchlin** and *P. Gardin*[#]

**von Karman Institute, Rhode-Saint-Génèse, Belgium*

***Laboratoire Transferts, Ecoulements, Fluides, Energétique, Pessac, France*

Institut de Recherche Sidérurgique, Maizières-Les-Metz, France

Abstract

This paper presents a macroscopic analysis of gas-jet wiping, with an emphasis on the comparison of the results provided by numerical simulations and experiments. The purpose of the study is to validate test cases that are reproducible in the laboratory, so as to be able to simulate numerically the air-knife coating process in hot-dip galvanizing. For the first time, the process is studied with small scale free surface simulations based on a Volume Of Fluid (VOF) approach coupled to a Large Eddy Simulation (LES) turbulence model. Single phase LES simulations of a plane impinging jet on a flat plate are first conducted, in order to provide a full characterization of the wiping jet. The effect of the substrate motion and presence of the liquid coating film on the pressure and shear stress distributions is analyzed. The interface of the film in the wiping region given by the two-phase simulation is then compared to the thickness profile yielded by an analytical model. The asymptotic film thicknesses after wiping are compared for a set of conditions, in the case of jet wiping with water. The splashing phenomenon, which is characterized by the ejection of droplets from the runback film flow, is finally investigated experimentally and numerically. The conditions leading to its occurrence are confronted, yielding encouraging results for the applicability of the numerical approach to the industrial process.

1 Introduction

Coating techniques are used in various industrial processes such as paper and photographic film manufacturing, wire coating and in the finishing of steel strips. In the dip coating method, the coating material is applied on the substrate in its liquid state. A continuous web is dipped into the coating fluid, and withdrawn so that one or both of the web sides are wetted. However, most of the time, the industrial requirements are such that the coating thickness has to be reduced and accurately controlled. Gas-jet wiping is one of the most popular techniques for that purpose, because it avoids a physical contact between the coating film and the doctor blade. In hot-dip coating, e.g. in the galvanization process, there is no other available technique. Jet wiping is based on the use of a turbulent slot jet (“air knife”) impinging on the dragged liquid film, leading to the formation of a runback flow to the bath, and the reduction of the film thickness (Figure 1). The wiping parameters are accurately set up in order to provide a thin and regular thickness. This mechanism is controlled by aerodynamic actuators, which are the mean pressure gradient and shear stress distributions induced by the jet on the liquid interface¹⁻³. A number of references in literature propose mathematical models for jet wiping flows. While some of them adopt an empirical approach of the process⁴⁻⁵, others provide analytical models describing the liquid film flow at a space scale smaller than the wiped film thickness^{1-3,6-7}. However, there has been no attempt until very recently⁸ to perform a two-phase numerical modelling of the process. The jet wiping process involves indeed highly coupled physical phenomena, due to the interaction between the turbulent gas jet and the laminar liquid film. The numerical techniques involved are developed in a related paper⁸.

In some operating conditions, the ejection of liquid droplets from the runback flow is observed; this phenomenon, referred to as splashing, is the physical limit of the wiping process. Yoneda⁹ attributes its origin to a combination of shearing off roll waves and undercutting, and derives a physical model for spray generation. A phenomenological model for its occurrence is also proposed by Buchlin¹⁰.

The aim of the present study is to model experimentally and numerically the gas jet-liquid film interaction in order to provide predictive tools for the estimation of the final film thickness after

wiping, and the conditions leading to splashing. For the first time, the wiping process is studied with two-phase numerical simulations, validated by experimental data. The small scale free surface simulations are based on a Volume Of Fluid (VOF) approach coupled to a Large Eddy Simulation (LES) turbulence model. On a practical point of view, the simulation of the two-phase flow allows validating macroscopic models predicting the mean film thickness after wiping for example, or the conditions leading to splashing. Those simplified models are used on production lines, e.g. galvanization lines, for the adjustment of the wiping conditions to reach a given coating quality^{7,11}.

In a first step, the emphasis is given to the study of the wiping actuators (mean pressure gradient and shear stress distributions) induced by a normal plane impinging jet on a dry fixed surface. Resulting typical profiles are shown in Figure 2. Such a study is of interest for the validation of the single phase LES simulation of the turbulent impinging jet, and the results are meant to be the inputs of an analytical model yielding the film thickness distribution in the wiping region. The effect of the substrate motion and the presence of the dragged liquid film on the actuators is analyzed numerically. The film interface given by the two-phase numerical modelling is then compared to the thickness distribution obtained with an analytical model, in which the boundary conditions in terms of pressure gradient and surface shear stress are the distributions previously found. The predicted and measured asymptotic film thicknesses after wiping are compared for a wide range of standoff distances L between the nozzle and the substrate (and constant jet Reynolds number). Finally, the occurrence of the splashing phenomenon is compared qualitatively between experiments and numerical simulations, and the conditions in which it appears are identified in both manner.

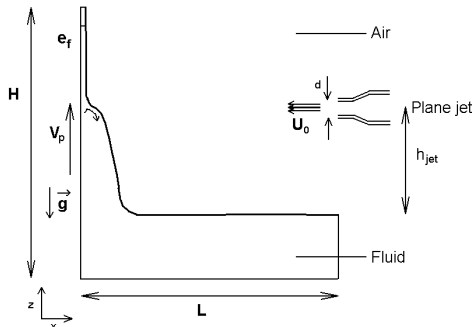


Figure 1: The jet wiping process

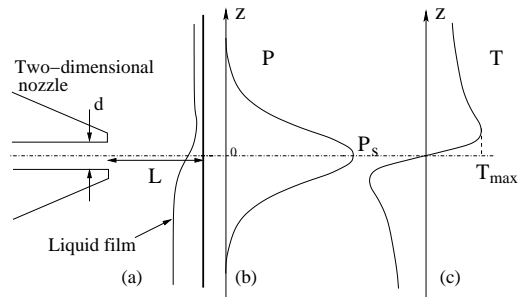


Figure 2: Sketch of the jet configuration: (a) Nozzle placement; (b) Typical impingement pressure profile; (c) Typical shear stress profile

In the following sections we first describe the numerical modelling of gas-jet wiping. The governing equations and the numerical methods are developed in section 2. Experimental techniques are then precisely described in section 3, followed by the development of a 1D analytical model for the film interface in section 4. Finally, the results obtained by numerical simulations are compared to those given by experiments and discussed in section 5. The single phase simulations are first validated with experimental data. The jet wiping mechanism and its main parameters are then analyzed with the two-phase flow simulations. In the last section, conclusions and perspectives are drawn.

2 Numerical modelling

The two-phase numerical modelling is described through the governing equations of the problem and the numerical methods used. The main numerical parameters are given.

2.1 Governing equations

The present work is restricted to isothermal two-phase flows of non miscible fluids with constant surface tension in a field Ω . In order to obtain a unique model for both the gas and liquid phase, a phase function C is introduced in the model to describe the interface evolution. After multiplying the incompressible Navier-Stokes equations in each phase by C , summing them on all phases and integrating the phase average variables over a characteristic volume, the governing equations for the two-phase flow are formulated as follows¹²:

$$\rho \left(\frac{\partial \vec{u}}{\partial t} + (\vec{u} \cdot \nabla) \vec{u} \right) = -\nabla p + \rho \vec{g} + \nabla \cdot \left((\mu + \mu_T)(\nabla \vec{u} + \nabla^T \vec{u}) \right) + \vec{F}_{ST} \quad (1)$$

$$\nabla \vec{u} = 0 \quad (2)$$

$$\frac{\partial C}{\partial t} + \vec{u} \cdot \nabla C = 0 \quad (3)$$

where ρ is the fluid density, μ its dynamic viscosity, \vec{g} the gravity vector, \vec{u} the velocity, t the time, p the dynamic pressure, and $\vec{F}_{ST} = \sigma \kappa \vec{n}_i \delta_i = \sigma \nabla \cdot (\nabla C) \frac{\nabla C}{\|\nabla C\|}$ is a source term for the normal stress due to the liquid/gas surface tension σ ¹³. \vec{n}_i is the normal vector to the free surface, and κ is the curvature of the interface.

The advection equation of the phase function C (3) characterizes the topological changes of the free surface as a material contact surface. In this way, it simultaneously models the evolution of fluid 0 (air) and 1 (liquid). In practice, the interface is described by $C=0.5$.

The model (1-3) is relevant to simulate the film dragging without the interaction with the turbulent jet, i. e. with $\mu_T = 0$. However, when turbulence develops, all the scales cannot be taken into account by the interfacial grid, if one wants to keep a reasonable computational cost. Therefore, an explicit turbulence model has to be added. A Reynolds Average Navier Stokes (RANS) model is not suitable in this case because of the unsteadiness of the free surface and the considered time and space scales. Large Eddy Simulation (LES) has been chosen, in which a turbulent viscosity μ_T (4) is added in equation (1) to model the dissipative effect of the small scale turbulent structures:

$$\mu_T = \rho (C_M \bar{\Delta})^2 \sqrt{2(\nabla \vec{u} \otimes \nabla \vec{u})} \quad (4)$$

where $\bar{\Delta}$ is the space filter, and C_M the mixed model constant, expressed as follows:

$$C_M = C_S^{2\eta} C_{TKE}^{1-\eta} \quad (5)$$

where η varies between 0 and 1, C_S is the Smagorinsky model constant and C_{TKE} the Turbulent Kinetic Energy (TKE) model constant. Typical values of these constants are $\eta = 0.5$, $C_S = 0.12$ and $C_{TKE} = 0.2$.

The LES model is based on a concept of scale separation in which the larger structures are solved (1-3) directly whereas the smaller ones are modelled (4-5). From a numerical point of view, the scale separation is carried out on the local space scale through spatial filtering by the computational grid. In equation (4), the spatial filter size $\bar{\Delta}$ is estimated by $\bar{\Delta} = \sqrt{\Delta x \Delta y \Delta z}$.

2.2 Numerical methods

On the basis of the Computational Fluid Dynamics library Aquilon¹⁴, the momentum equation (1) is approximated by a finite volume spatial discretization on a fixed staggered Cartesian grid over the whole computational domain. The time discretization and the coupling between

velocity and pressure are achieved with a minimization algorithm based on an augmented Lagrangian method¹⁵⁻¹⁶. For the space derivative of (1), the advection terms are discretized by a hybride scheme of Patankar¹⁷ whereas a centered scheme is used for the other terms. A Continuum Surface Force (CSF) model¹³ is implemented for the treatment of the surface tension effects. The implicit discretization implies the numerical solving of a linear system, which is achieved thanks to an iterative procedure of Bi-Conjugate Gradient Stabilized II (Bi-CGSTAB) of van der Vorst¹⁸. The Bi-CGSTAB is preconditioned under a Modified and Incomplete LU method¹⁹. In the present study, a geometric Piecewise Linear Interface Construction (PLIC) VOF method and a mathematic Total Variation Diminishing (TVD) VOF approach²⁰ were performed to treat interface advection. These numerical methodologies have already been validated on several scalar advection and free surface problems^{20,21}.

2.3 Boundary conditions and grid requirements

An irregular Cartesian grid was implemented for the computations, which typically contains 19200 points (150×128), and is presented in Figure 3. It is strongly refined at the interface along

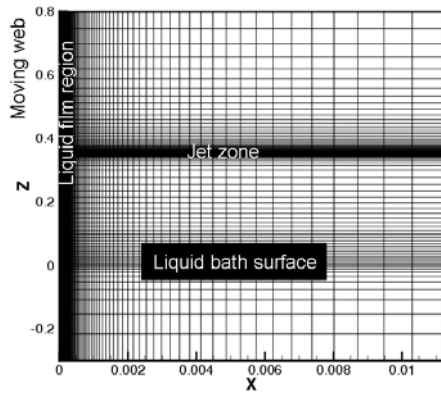


Figure 3: Typical mesh

the plate and at the bath free surface. Grid clustering is also performed along the jet axis, the LES model requiring a better description of the flow in the zones of higher turbulence and shear stress. In order to capture all the physical processes leading to turbulence (and for the estimation of the shear stress at the wall), the y^+ of the first cell is 1 (3.5 μm). The boundary conditions are a wall condition at the bottom of the domain, Neumann conditions at the top and right side, and a sliding condition at the left (velocity V_p). The jet on the right is introduced with a “top-hat” velocity profile based on experimental measurements²².

3 Experimental techniques

The experimental techniques used are described here, together with their accuracy.

3.1 Normal jet impingement

This first step in the experimental study allows the characterization of the air nozzle used for the jet wiping investigation. The aim is to measure the mean pressure and shear stress profiles induced by the two-dimensional jet impinging normally on a flat fixed plate. For that purpose, the apparatus consists of a two-dimensional air jet created by a 0.6 m long slot nozzle which is impinging on a 0.65×0.30 m aluminium plate (Figure 4). The plate is mounted on a vertical displacement system with a precision of 2 μm . For the measurements, the nozzle is kept stationary while the plate is moved manually with a given spatial step. The plate can also be moved with a screw in order to adjust the standoff distance L between the plate and the nozzle. The nozzle air supply is provided by a single-stage 14 kW centrifugal blower. The nozzle slot opening for all the experiments is $d=1.4$ mm. The turbulence intensity at the exit of the jet is 2.5% at the jet Reynolds number $Re=4500$. The impinging plate is instrumented with a static pressure hole of 0.5 mm of diameter to measure the pressure at impingement. For the shear stress, it was decided to use a simplified Stanton probe, as proposed by Hool²³. It is made of a thin razor blade whose tapered cutting edge is positioned over a static pressure hole, leaving an open space δx with respect to the hole's edge. It is sticken on the plate with a layer of cyanocrylate glue having a negligible thickness with respect to the one of the blade. It forms a

total pressure probe of physical size h ($2h=150\ \mu\text{m}$ being the total thickness of the razor blade), lying within the effective height at which the measured shear stress corresponds to a linear wall velocity profile. By measuring the difference between the static pressure in a close location and the total pressure from the Stanton probe, one obtains the dynamic pressure which is directly related to the wall shear stress.

The pressure signals are measured thanks to membrane pressure transducers. The data acquisition is performed on a personal computer equipped with a Testpoint[®] card. A program was developed to acquire periodically the pressure signal, leaving enough time for the moving of the plate to its next position. The spatial step is 0.2 mm, and the acquisition frequency is 2 kHz. The uncertainty on the pressure gradient is estimated to 4%. The uncertainty on the shear stress is about 5% in the wall jet region. In the stagnation region ($z/d \leq 1.4$), the severe favourable pressure gradient is beyond the limiting conditions recommended by Patel²⁴ for a maximum error of 6% on the shear stress (the Stanton probe is calibrated in zero-pressure gradient channel flows). Therefore, the uncertainty for $z/d \leq 1.4$ is expected to be at least 10%.

3.2 Jet wiping

In the jet wiping experiments, the mean film thickness after wiping is measured, and the conditions leading to the occurrence of the splashing phenomenon are detected. The test facility which was used for that purpose is shown in Figure 4. It includes a vertical rubber strip 5 m long and 0.5 m wide, stretched between two rolls. The strip is set into motion by the upper roll, which is entrained by an electric motor. The strip velocity, which can be adjusted precisely in the range 0.5 to 5 m/s, is measured by means of a tachometer. The lower roll is fixed to a mechanical displacement system allowing the adequate stretching of the strip. It dips into a bath of water to which a small concentration of surfactant was added, to ensure a good wettability of the strip. The nozzle is positioned perpendicularly to the strip. The nozzle is sufficiently long to avoid edge effects, and it is fed up to 8 kPa with a blower similar to the one mentioned before. For sake of simplicity, the wiping mechanism is studied only on one side of the strip. To ensure a good stability of the strip in the impact region of the jet, the rear face is sliding on an aluminum plate lubricated by the entrained water. The distance L between the nozzle and the strip is tuned using shims. The liquid film mean thickness h_f is determined through the flow rate measured by weighting the liquid collected at the top of the strip during a time elapse. The film is withdrawn at the top of the band by the action of a rubber scraper combined to a vacuum cleaner based on 4 bars air ejectors. Two lateral small jets draw the liquid film towards two suction ports which are connected to a cyclone. A balance measures the amount of the collected water while the weighting time is controlled by a chronometer. The measurements of the film thickness h_f are reproducible within 3% in average, which is the order of magnitude of the uncertainty on h_f .

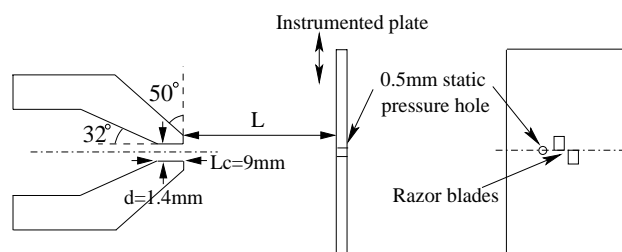


Figure 4: Wiping nozzle and impingement plate

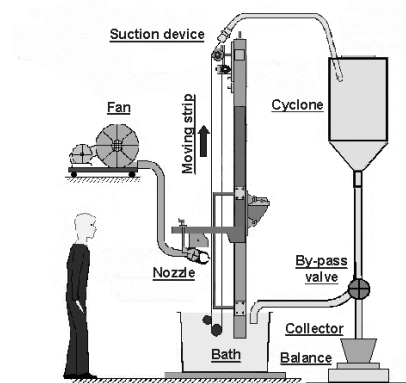


Figure 5: Gas-jet wiping facility

Splashing is detected from visual observation, but it can also be associated with a drop of the wiping efficiency. For a nozzle pressure P_n , the strip velocity is gradually increased until splashing occurs. For all the splashing experiments, we will consider only the apparition. Although visual detection is bound to the experimentalist's subjectivity, it is reproducible at 2%, while the uncertainty is 8%.

4 Analytical model of film thickness

Several models for the film interface in jet wiping are proposed in literature^{1-3,7}, with different levels of solutions. The theoretical description of gas-jet wiping usually relies on the lubrication approach, which assumes negligible inertia with respect to viscous, gravity and pressure terms. The (Oz) momentum equation of the film states that the shear stress balances the weight and pressure, and the boundary conditions express the no-slip condition of the film on the substrate, and the continuity of shear stress at the free surface. The resulting flow rate equation has the following non-dimensional form:

$$\Gamma \frac{d^3 \hat{h}(Z)}{dZ^3} = 1 + \nabla \hat{P}(Z) + \frac{2Q - 3\hat{h} - 1.5\hat{T}\hat{h}^2}{\hat{h}^3} \quad (6)$$

where $\nabla \hat{P}$ and $\hat{T}(Z)$ are respectively the pressure gradient and shear stress distributions of the jet at impingement. \hat{h} and Q are the local film thickness and flow rate. The normalized variables are defined as follows: $Z = z/d$, $\hat{h} = h/h_0$ with $h_0 = \sqrt{\mu_1 U / \rho_1 g}$, $\Gamma = \sigma h_0 / \rho_1 g d^3$, $Q = q/q_0$ with $q_0 = 2/3 V_p h_0$, $\nabla \hat{P} = \nabla P / \rho_1 g + 1$, and $\hat{T} = \tau / \tau_0$ with $\tau_0 = \sqrt{\mu_1 V_p \rho_1 g}$. Subscript 0 refers to the dragged liquid film without jet wiping, and 1 refers to the liquid phase properties.

Equation (6) has two unknowns, \hat{h} and Q , and the continuity equation is needed for its solving. A simplified model can be derived from (6), assuming a negligible effect of surface tension:

$$(1 + \nabla \hat{P}) \hat{h}^3 - 1.5 \hat{T} \hat{h}^2 - 3\hat{h} + 2Q = 0 \quad (7)$$

The solution of (7) is obtained by solving locally the cubic equation, using the pressure gradient and shear stress distributions $\nabla \hat{P}$ and $\hat{T}(Z)$ given by numerical simulation of the impinging jet. A zero-dimensional model (hereafter referred to as the Knife Model) can be derived from (7) if one postulates that the wiping mechanism is the result of the first maximum jet pressure gradient and maximum shear stress. This approach assumes implicitly that both quantities act at the same location X_{opt} (which is very close to reality²⁵) and that surface tension has no effect on the final film thickness. With such an approximation, the film equation reduces to the simple algebraic equation:

$$(1 + \nabla \hat{P}_{\max}) \hat{h}_{opt}^3 - 1.5 \hat{T}_{\max} \hat{h}_{opt}^2 - 3\hat{h}_{opt} + 2Q_{opt} = 0 \quad (8)$$

Since there are two unknowns, \hat{h}_{opt} and Q_{opt} , a second equation is needed. It is derived by stating that the wiping efficiency corresponds to the optimum final net flow rate, so that:

$$\hat{h}_{opt} = \frac{\hat{T}_{\max} + \sqrt{\hat{T}_{\max}^2 + 4(1 + \nabla \hat{P}_{\max})}}{2(1 + \nabla \hat{P}_{\max})} \quad (9)$$

The flow rate Q can then be determined from (8), and it gives readily the final film thickness after wiping h_f .

5 Results

Numerical simulations and experiments are used to provide results on normal impinging jets and jet wiping. These results are compared and discussed in the following section.

5.1 Jet impingement on dry and wet surfaces

It has been known since long that the wiping mechanism is controlled by the mean pressure gradient and shear stress distributions at impingement¹⁻³. The study of the normal impinging jet on a dry surface is therefore relevant for a preliminary characterization of the jet. The effect of the substrate motion and the presence of the liquid film on the distributions are then analyzed numerically since this task cannot be made experimentally. The conditions chosen for the validation of the numerical results are $Re=4500$, $d=1.4$ mm and $L/d=8$.

5.1.1 Jet impingement on a dry fixed surface

The plane turbulent impinging jet is a widely used test case for numerical simulations. Numerous studies in literature provide confrontations of numerical and experimental results in terms of mean pressure at impingement^{11,26-29}. Such comparisons are not so systematic as far as the shear stress is concerned. It is however useful in a first step to validate the single phase jet LES simulations, and on the other hand, the shear stress and pressure gradient at impingement are necessary inputs for the analytical model described in section 4.

One can observe in Figure 6a an excellent agreement between the normalized pressure gradients $\nabla P/P_n \cdot d$ (where P_n is the jet pressure).

The comparison of the numerical and experimental shear stress is not so simple. From a numerical point of view, as the first cell at the wall ($3.5 \mu\text{m}$) lies within the viscous sublayer, the shear stress computed at this height is not dependent on the computation. As it can be seen in Figure 6b, the qualitative shape of the distributions compares well, but the numerical values are up to 40% higher than the experimental ones at the peak position ($z/d \approx 1.2$). The difference drops to about 25% in the wall jet region ($z/d \geq 4.5$). It can be explained by the fact that the calibration law of the Stanton probe, which is established in zero-pressure gradient flows channel flows, is not valid around the stagnation point. Moreover, the experimental underestimation of shear stress is all the more important as the physical size of the probe is large³¹. An encouraging agreement is obtained if the shear stress is computed at $25 \mu\text{m}$ from the wall, which corresponds to $y^+=7$. At $75 \mu\text{m}$ (which corresponds to the physical height of the Stanton probe), the experimental shear stress is strongly underestimated in the stagnation zone, while it is rather well predicted in the wall jet region.

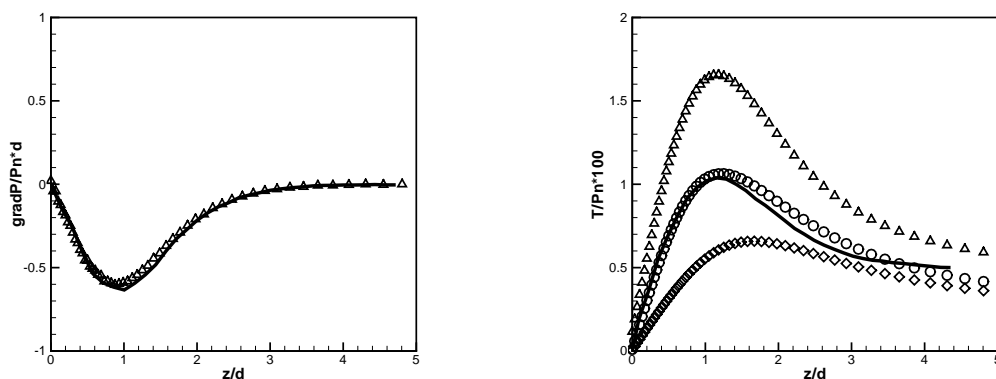


Figure 6: Impingement on a dry fixed plate

- (a) Pressure profile- line: experiment, Δ : simulation
(b) Shear stress profile- line: experiment, Δ : simulation ($3.5 \mu\text{m}$), \circ : simulation ($25 \mu\text{m}$), \diamond : simulation ($75 \mu\text{m}$)

5.1.2 Jet impingement on a moving surface

The effect of the substrate motion on the pressure gradient and shear stress distributions is now analyzed. The substrate motion is towards the positive z and the plate velocity is fixed at $V_p=1.55$ m/s. To properly compare the profiles with the ones on a dry fixed surface, all of them have been shifted to 0 at the stagnation point.

As depicted in Figure 7a, the plate motion has a negligible effect on the pressure gradient profile. That could be expected since the velocity ratio (jet exit velocity/substrate velocity) U_0/V_p is as high as 40.

As for the shear stress, the movement of the plate does have a slight effect on its distribution (Figure 7b), which becomes asymmetric (Figure 8). The slipping effect on the film surface involves an increase of the peak value $|T_{\max}|$ of 6.5% on the negative z side. The wall jet air flow is indeed opposed to the substrate motion, resulting in an increase of the velocity gradient. The energy conservation implies that the peak to peak shear stress value remains constant whatever the substrate velocity is.

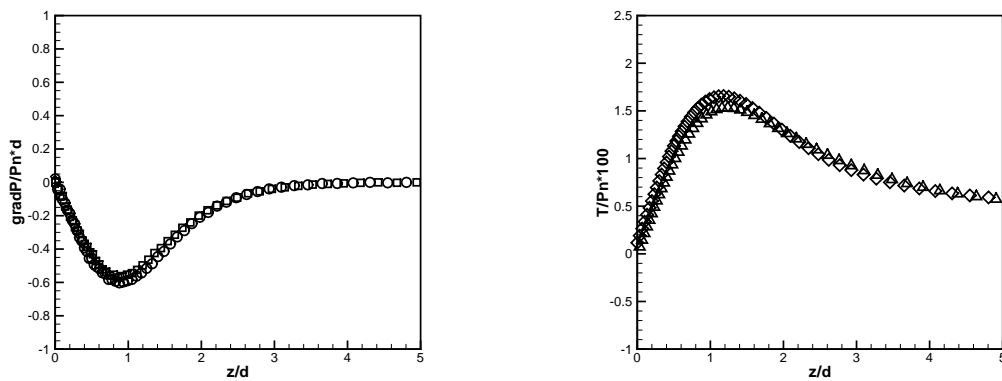


Figure 7: Impingement on moving and fixed plates

(a) Pressure profile - \square : simulation on a moving plate, \circ : simulation on a fixed plate
 (b) Shear stress profile - line: Δ : moving plate, \diamond : fixed plate

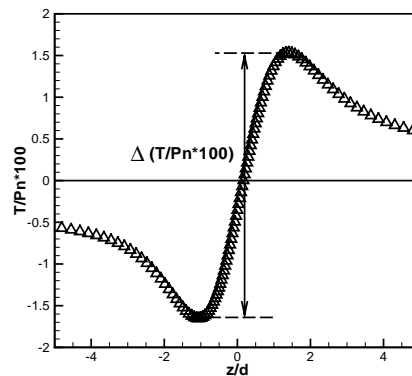


Figure 8: Shear stress profile - Δ : simulation on a moving plate

5.1.3 Jet impingement on a moving film

The effect of the presence of the wiped liquid film together with the substrate motion is now investigated. The liquid is water, with a surface tension of 0.03 N/m due to the surfactant.

The presence of the liquid film affects more or less the pressure gradient profiles, depending on the flow region (Figure 9a). At the peak location, it is about 25% lower. The pressure gradient taken in the liquid film at the moving wall is a little higher (in absolute value) than the one at the interface (in the gas phase); the small difference proves that the thin film approximation

made in section 4 was valid. The locations at which slightly larger differences appear ($0.4 \leq z/d \leq 1$ and $z/d \approx 2.4$) correspond to the zones where the interface shows up a higher curvature radius. The difference lies in the surface tension term which is proportional to the film curvature $\partial^2 h / \partial y^2$. One should also keep in mind that an uncertainty of the order of $\Delta x / 2$ can be associated with the way of locating the interface, since only the volume fraction in each computational cell is known.

As shown in Figure 9b, the shear stress is more affected by the presence of the liquid film. When calculated at the interface, it is up to 30% (at the peak location) lower than the one taken on a dry plate, moving or not. This is probably due to the sliding property of the interface and the higher curvature of the liquid film at the location of T_{\max} . The difference is indeed much lower in the wall jet region. Numerically, measuring a shear stress at a gas-liquid interface remains a tricky problem, and a large uncertainty can be associated to it. In our case, the normal vector to the interface is estimated by $\vec{n}_i = \nabla C / \|\nabla C\|$ and the normal velocity by $\vec{u} \cdot \vec{n}_i$. Its tangential component is deduced from $\vec{u} \cdot \vec{t}_i$, and $\mu \cdot \partial \vec{u} \cdot \vec{t}_i / \partial \vec{t}_i$ is the shear stress at the interface.

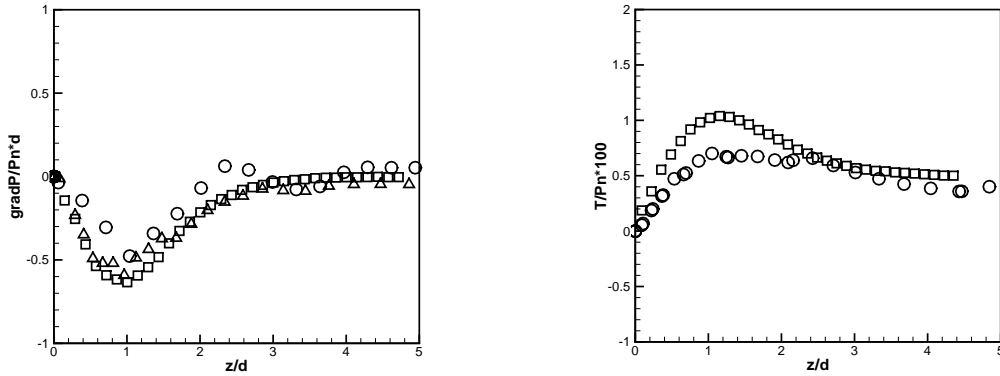


Figure 9: Impingement on a dry fixed plate:

- (a) Pressure profiles \square on a fixed plate, Δ on a moving plate dragging a liquid film (liquid phase), \circ at the interface of the dragged liquid film (gas phase)
- (b) Shear stress \square on a fixed plate, \circ at the interface of the dragged liquid film (gas phase)

The pressure gradient and shear stress profiles are meant to be injected in the one-dimensional model described in section 4. For sake of simplicity, those distributions are usually chosen as the ones obtained on a dry fixed plate¹¹. It has to be studied to which extent the variations of the pressure gradient and shear stress distributions affect the results of the 1D-model.

5.2 Jet wiping

The complete gas-jet wiping process is now analyzed. The shape of the computed film interface in the wiping region is first compared to the analytical one. A parametric study on the effect of the nozzle to plate distance on the asymptotic thickness is then carried out. The splashing phenomenon is finally observed and quantified by both the numerical and experimental method.

5.2.1 Shape of the film interface in the wiping region

The shape of the simulated interface is now compared to the thickness profile yielded by the analytical model described in section 4. The sensitivity of the model to the ∇P and T profiles is checked by comparing the results when the inputs are respectively the distributions found numerically on a dry fixed plate, on a moving plate, and on a moving plate dragging a liquid film. The comparison of the thickness profiles thus obtained is made in Figure 10a. The close view of the region downstream the wiping jet (Figure 10b) shows that the film thickness after

wiping is underestimated when the ∇P and T inputs are the profiles computed on a dry still or moving plate. The difference with the interface obtained numerically reaches 15%, while the substrate motion induces a negligible variation on h_f with respect to the dry plate. If ∇P and T are now the ones computed on the film interface, then h_f is overestimated of 35%. The high uncertainty on those profiles might explain the difference.

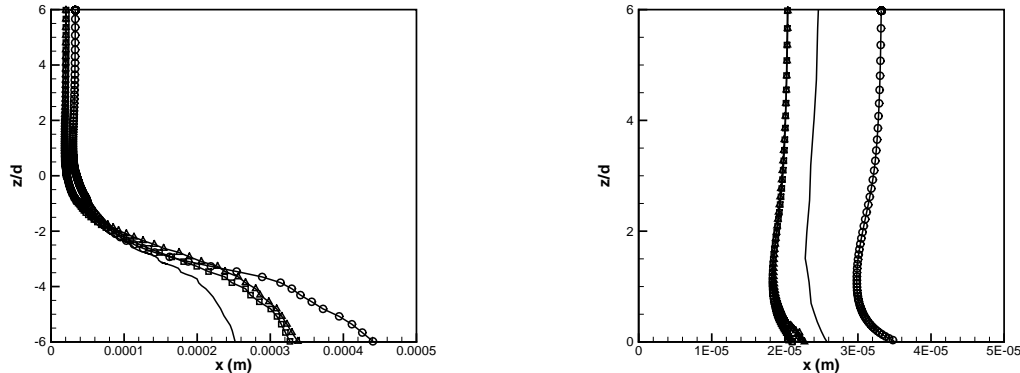


Figure 10: (a) Comparison of the interface yielded by the 1D-model with different inputs, and the one obtained by simulation (b) Close view of the interface in the region downstream the jet
– o: 1D model, with film, Δ : 1D model, moving plate, \square : 1D model, dry fixed plate, line: simulation

Upstream the impinging zone, the runback flow from the 1D-model is thicker than the simulated profile, with ∇P and T on dry, moving, or moving wet plate. A reason could be the diffusivity of the schemes in the simulation when the size of the grid cells is large and the mesh is very irregular; it is the case in this zone, described by less points than the impinging zone. On the other hand, the lubrication assumption made in the analytical model is probably not valid in the runback flow region, where the velocity may not be unidirectional. Moreover, the model is very sensible to the pressure gradient in the region $z/d \leq -4$: its reduction of up to 65% involves a runback flow film thickness up to 35% larger. Its sensibility to the upstream maximum pressure gradient is comparatively weaker: an increase of 60% results in a reduction of 16% of the final film thickness.

The analytical model, when supplied with the pressure gradient and shear stress profiles computed on a dry fixed plate, gives results in reasonable agreement with the interface obtained numerically. The film thickness after wiping tends to be underestimated though. If the actuators are taken at the film interface, their high uncertainty strongly affect the final thickness profile.

5.2.2 Asymptotic thickness and influence of the nozzle to plate distance

Experimental data is now used to validate the numerical tool for the prediction of a macroscopic parameter, the film thickness after wiping h_f . Its evolution with the standoff distance L/d , i. e. the ratio between the nozzle to plate distance and the nozzle width of the jet is analyzed for the range $2 \leq L/d \leq 12$. The nozzle slot opening is kept constant while the nozzle to plate distance is modified. The effect of L/d is investigated for a film Reynolds number Re_f ranging from 30 to 52 and for a constant jet Reynolds number $Re=4500$. Figure 11 shows that the asymptotic thicknesses obtained by simulation compare well to the experimental ones within the experimental accuracy, except for L/d lower than 4, for which the simulated thicknesses are much lower. As mentioned by Babu et al.³⁰, this difference is attributable to the artificial confinement induced by the boundaries of the numerical domain or the absence of flow entrainment, since the nozzle is located at the boundary. The Knife model gives good predictions for the whole L/d range. The zero-dimensional model was supplied with correlations for the maximum pressure gradient and shear stress based on experimental data²⁹. It allows

retrieving the thickness plateau found experimentally for $2 \leq L/d \leq 8$; this operating range is interesting for jet wiping since the thickness weakly depends on the standoff distance.

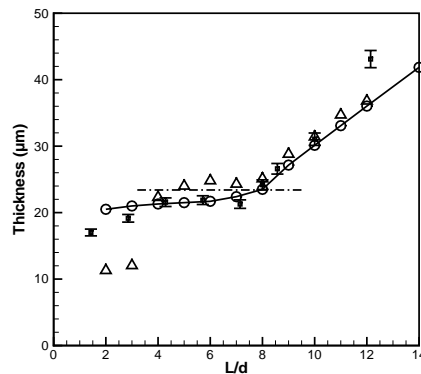


Figure 11: Influence of L/d on the film thickness after wiping, \square : experiments, Δ : simulation, \circ : Knife model, dotted line: plateau

5.2.3 Splashing

In certain wiping conditions, a phenomenon of wrenching of drops from the runback flow can appear: it is the physical limit of applicability of gas-jet wiping. This phenomenon is called splashing and it harms seriously the correct operation of the process since the ejected liquid droplets may seal the slot opening of the air jet. It is thus important to be able to predict its occurrence. The major parameters involved in this phenomenon have been identified and modelled by Buchlin et al.^{7,10}. The aim of this study is to validate the numerical tool for the predictions of wiping conditions leading or not to splashing.

In practice, splashing is systematically initiated on the strip edges where some droplets are ejected from the runback flow, and it propagates along the strip width until a complete explosion of the film occurs. An external perturbation can also trigger splashing close to critical conditions. Fully developed splashing is illustrated in Figure 12a, and it compares qualitatively well with the film interface obtained numerically in splashing conditions (Figure 12b).

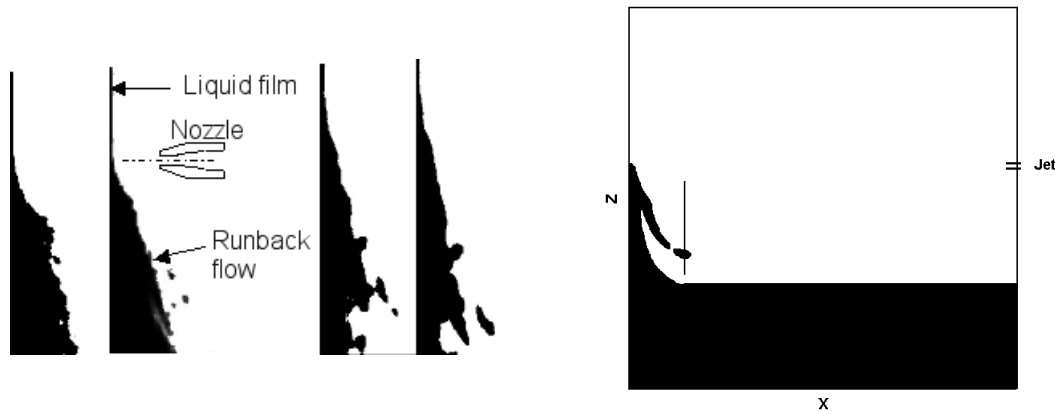


Figure 12

(a) Experimental high speed visualization of fully developed splashing on the wiping facility, side view (1000 FPS, $L/d=10$, $V_p=3.5$ m/s)
 (b) Typical interface shape in two-phase flow modelling ($L/d=8$, $V_p=1.55$ m/s, $z/x=78$), and position of the droplets counter (vertical line)

Numerical simulations are performed for substrate velocities slightly above and below the critical velocity found experimentally. A counter of the ejected droplets volume is added to

detect splashing in the unsteady simulations. Its position in the computational domain is shown in Figure 12b. A typical evolution of the rate of ejected liquid through the counter is shown in Figure 13. During the first 0.4 sec, the sudden interaction between the liquid film and the jet induces a wrench of drops, which has nothing to do with splashing. After this transition time, the liquid rate remains equal to 0 until the end of the considered period (1 sec). This evolution is compared to a second one in which the velocity is suddenly increased from 2 m/s to 4 m/s at the time $t=0.5$ sec. The dotted line in Figure 13 shows a significant increase of the liquid rate around 0.65 sec, which persists until the end of the simulation. We then consider splashing appears for a strip speed V_p of 4 m/s. This typical time evolution of the counter with and without splashing shows there is no ambiguity on the detection of the phenomenon as soon as the mass of liquid ejected remains different from 0 for long times.

The comparison of numerical and experimental results in Figure 14 shows an excellent agreement within the experimental uncertainty. These results constitute an encouraging first step in proving that the numerical tool is perfectly reliable for the prediction of splashing in more practical configurations.

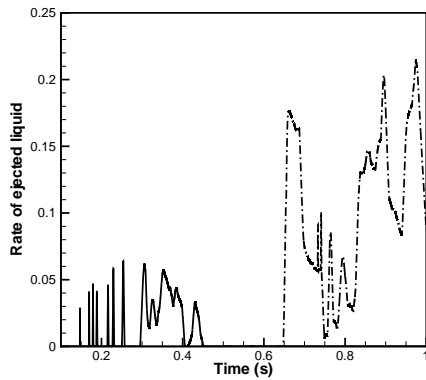


Figure 13: Rate of ejected liquid for two strip speeds – solid line: $V_p=2$ m/s, dotted line: $V_p=4$ m/s

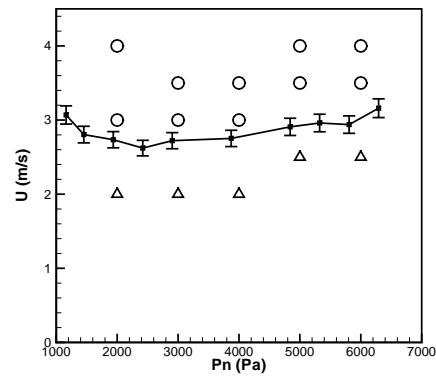


Figure 14: Validation of the critical velocity for splashing occurrence - \square : experimental critical velocity, Δ : simulation, no splashing, \circ : simulation, splashing

6 Conclusions

The jet-wiping process has been analyzed, with an emphasis on its application in the galvanization process. For that purpose, the interaction between the turbulent plane jet and the liquid film has been studied, using simultaneously an interface tracking simulation tool coupled with a Large Eddy Simulation model, and experiments. In addition, a one dimensional macroscopic model, which requires input parameters such as the shear stress and pressure gradient profiles at the interface, is proposed for predicting the interface shape in the wiping region. The complementarity of the various approaches allows demonstrating the good qualitative and quantitative agreement between the numerical and experimental results.

The first step of the study consists in the characterization of the wiping actuators, i.e. the mean pressure gradient and shear stress induced by the plane jet on a flat plate. The experimental and numerical profiles have been successfully compared. The simulations show that the substrate motion has very little effect on the distributions, whereas the presence of the liquid film leads to larger differences and more noisy profiles

The implementation of the numerical data in the 1D macroscopic model shows that the interface profiles in the wiping zone could be well predicted provided that an appropriate model for the wiping actuators is used.

The two-phase flow simulations allow the determination of the final film thickness after wiping. The values are in reasonable agreement with experimental results, except for high confinements. Besides, the Knife model is demonstrated to be a good estimator for the final thickness, and

much less time consuming than numerical simulations. Finally, the occurrence of splashing in the simulations compares qualitatively well with experiments, and the critical conditions identified in both way are in good agreement.

Solving the Navier Stokes equations in an eulerian volume of fluid framework has been demonstrated to be a valid way of modeling jet wiping. The work of validation performed here is a first step in the applicability of the numerical tool in industrial conditions. Its advantage is the possibility to check rapidly the effect of various parameters (e. g. nozzle geometry) on the jet wiping process for its optimization.

6 References

1. Thornton, J.A., Graff, M.F., 1976, An analytical description of the jet finishing process for hot-dip metallic coating on strip, *Metallurgical Trans. B*, **7B**, 607-618.
2. Tuck, E.O., 1983, Continuous coating with gravity and jet stripping, *Phys. Fluids*, **26**, 2352-2358.
3. Ellen, C.H., Tu, C.V., 1984, An analysis of Jet Stripping of Liquid Coatings, *J. Fl. Eng.*, **106**, 399-404.
4. Tu, C.V., 1990, Optimization of lip gap for thin film coating in the jet stripping process, *5th Int. Conf. on Manufacturing Eng. Proc.*, Wollongong, 155-159.
5. Naphade, P., Mukhopadhyay, A., Chakrabarti, S., 2005, Mathematical modelling of jet finishing process for hot-dip zinc coatings on steel strip, *ISIJ*, **45(2)**, 209-213.
6. Takeishi, Y., Yamauchi, A., Miyauchi, S., 1995, Gas wiping mechanism in hot-dip coating process, *ISIJ*, **81(2)**, 47-52.
7. Buchlin, J.M., 1997, Modeling of gas-jet wiping, *Thin Liquid Films and Coating Processes, VKI Lecture Series*, von Karman Institute for Fluid Dynamics.
8. Lacanette, D., Vincent, S., Arquis, E. and Gardin, P., 2005, Numerical Simulation of Gas-Jet Wiping in Steel Strip Galvanizing Process, *ISIJ Int.*, **45(2)**, 214-220.
9. Yoneda, H., Scriven, L.E., 1994, Analysis of spray generation in air-knife coating, *7th Symp. Coating Proc. Sc. and Tech. at the AIChE Spring. Nat. Meet.*, Atlanta, GA.
10. Buchlin, J.M., Gosset, A., Perrot, V., Dubois, M., Anthoine, J., 2003, Effect of nozzle angle on splashing in jet wiping, *Advances in Coating and Drying of Thin Films-ECS-03 Proc.*, Fribourg, Switzerland.
11. Hrymak, A.N., Forbes, J.F., Knight, J., Elsaadawy, E., Balthazaar, A., Sheng, Y., 2002, Air knife coating in hot-dip galvanizing, *44th MWSP Conf. Proc.*, **Vol. XL**, ISS, Warrendale, PA, 853-861.
12. Magnaudet, J., Eames, I., 2000, The motion of high-reynolds number bubbles in homogeneous flows, *Annu. Rev Fluid Mech.*, **32(1)**, 659-708.
13. Brackbill, J.U., Kothe, B.D., Zemach, C., 1992, A continuum method for modelling surface tension, *J. Comput. Phys.*, **100**, 335-354.
14. <http://www.trefle.u-bordeaux.fr/aquilon/index.html>
15. Fortin, M, Glowinski, R., 1982, Méthode de Lagrangien augmenté, Application à la résolution numérique des problèmes aux limites, *Collection méthodes mathématiques de l'informatique*, DUNOD, Paris.
16. Vincent, S., Caltagirone, J.P., 2000, A One-Cell Local Multigrid Method for Solving Unsteady Incompressible Multiphase Flows, *J. Comput. Phys.* **163**, 172-215.
17. Patankar, S.V., 1980, Numerical Heat Transfer and Fluid Flow, Hemisphere Publishing Corporation, New-York (U.S.A).
18. Van Der Vorst, H.A., 1992, Bi-CGSTAB: a fast and smoothly converging variant of Bi-CG for the solution of non-symmetric linear systems, *SIAM J. Sci. Stat. Comput.*, **13**, 631-644.
19. Gustafsson, I., 1978, On first and second order Symmetric factorization methods for the solution of elliptic difference equations, Chalmers University of Technology.
20. Vincent, S., Caltagirone, J.P., 1999, Efficient solving method for unsteady incompressible interfacial flow problems, *Int. J. Numer. Meth. Fluids*, **30**:795-811.
21. Vincent, S., Caltagirone, J.P., 2000, A One-Cell Local Multigrid Method for Solving Unsteady Incompressible Multiphase Flows, *J. Comput. Phys.*, **163**, 172-215.

22. Maurel, S., Sollicec, C., 2001, A turbulent plane jet impinging nearby and far from a flat plate, *Exp. in Fluids*, **31**, 687-696.
23. Hool, J.N., 1956, Measurement of Skin Friction using Surface Tubes, *Aircraft Eng.*, **28**, 52-54.
24. Patel, V.C., 1965, Calibration of the Preston Tube and Limitations of its Use in Pressure Gradients, *J. Fluid Mech.*, **23**, 185-206.
25. Tu, C.V., Wood, D.H., 1996, Measurements Beneath an Impinging Plane Jet, *Exp. Th. Fl. Sc.*, **13**, 364-373.
26. Wolfshtein, M., 1970, Some solutions to the the plane impinging jet, *Trans. ASME, J. Basic Eng.*, **92D**, 915-922.
27. Hwang, C.J., Liu, J.L., 1989, Numerical study of two-dimensional impinging jet flow fields, *AIAA J.*, **27(7)**, 841-842.
28. Bouainouche, M., Bourabaa, N, Desmet, B., 1997, Numerical study of the wall shear stress produced by the impingement of a plane turbulent jet on a plate, *Int. J. Num. Methods*, **7(6)**, 548-564.
29. Gosset, A., Buchlin, J.M., Rambaud, P., Dubois M., Modeling of gas-jet wiping at small standoff distances, *to be presented at the 6th European Coating Symposium*, Bradford, Great Britain, 2005.
30. Babu, P.C., Mahesh, K., 2004, Upstream entrainment in numerical simulations of spatially evolving round jets, *Phys. Fluids*, **16(10)**, 3699-3705.
31. Tu, C.V., Wood, D.H., 1996, Measurements beneath an impinging plane jet, *Exp. Th. Fluid Sc.*, **13**, 364-373.